Hindawi Publishing Corporation
Journal of Chemistry
Volume 2013, Article ID 437309, 10 pages
http://dx.doi.org/10.1155/2013/437309

Research Article

Synthesis and Performance of an Acrylamide Copolymer Containing Nano-SiO_2 as Enhanced Oil Recovery Chemical

Zhongbin Ye,[1,2] Xiaoping Qin,[1,2] Nanjun Lai,[1,2] Qin Peng,[2] Xi Li,[2] and Cuixia Li[3]

[1] *State Key Laboratory of Oil and Gas Reservoir Geology and Exploitation, Southwest Petroleum University, Chengdu 610500, China*
[2] *College of Chemistry and Chemical Engineering, Southwest Petroleum University, Chengdu 610500, China*
[3] *Department of Petroleum Chemical Engineering, Karamay Vocational & Technical College, Karamay 833600, China*

Correspondence should be addressed to Xiaoping Qin; 948801727@qq.com and Nanjun Lai; 29511393@qq.com

Received 4 April 2013; Revised 9 July 2013; Accepted 12 August 2013

Academic Editor: Ibnelwaleed Ali Hussien

A novel copolymer containing nano-SiO_2 was synthesized by free radical polymerization using acrylamide (AM), acrylic acid (AA), and nano-SiO_2 functional monomer (NSFM) as raw materials under mild conditions. The AM/AA/NSFM copolymer was characterized by infrared (IR) spectroscopy, ^{1}H NMR spectroscopy, elemental analysis, and scanning electron microscope (SEM). It was found that the AM/AA/NSFM copolymer exhibited higher viscosity than the AM/AA copolymer at 500 s^{-1} shear rate (18.6 mPa·s versus 8.7 mPa·s). It was also found that AM/AA/NSFM could achieve up to 43.7% viscosity retention rate at 95°C. Mobility control results indicated that AM/AA/NSFM could establish much higher resistance factor (RF) and residual resistance factor (RRF) than AM/AA under the same conditions (RF: 16.52 versus 12.17, RRF: 3.63 versus 2.59). At last, the enhanced oil recovery (EOR) of AM/AA/NSFM was up to 20.10% by core flooding experiments at 65°C.

1. Introduction

Polymer flooding plays an important role in the field of enhanced oil recovery (EOR) [1, 2]. However, the current widely used polymers, polyacrylamide (PAM) and partially hydrolyzed polyacrylamide (HPAM), cannot completely meet the requirements due to the hydrolysis, degradation, and others under high temperature or high salinity [3–6]. Furthermore, PAM and HPAM have poor shear resistance [2–7]. Polymer molecular chains will be cut off when polymer solution passes through the pump, pipeline, perforation, and porous medium at high speed, so the viscosity of polymer solution will be greatly reduced [1, 7, 8].

Recently, many studies have demonstrated that performance of composite material could be significantly improved by combination or copolymerization with a functional monomer containing nano-SiO_2. The composite material containing Nano-SiO_2, such as polyethylene terephthalate [9], styrene butadiene rubber [10], polyaniline [11], polyimide [12], and nylon 6 [13], may exhibit more satisfactory thermal stability, toughness, and strength owing to the effect of physical adsorption, hydrogen bond, Si–O bond, and C–Si bond [10, 12, 14–16]. However, there are no papers about the application of nano-SiO_2 in polymer for flooding to develop temperature tolerance, salt tolerance, and shear resistance of copolymer.

Keeping in mind these fundamental conditions, herein, a novel nano-SiO_2 functional monomer (NSFM; see Scheme 1) was introduced into AM/AA copolymer aiming to obtain satisfying temperature tolerance, salt tolerance, and shear resistance [17–20].

2. Experimental

2.1. Chemicals and Reagents. Ethanol (C_2H_5OH, ≥99.7%), ammonia (NH_4OH, 28.0%), vinyltriethoxysilane (VTES, ≥98.0%), acrylic acid (AA, ≥99.5%), acrylamide (AM, ≥99.0%), sodium hydrogen sulfite ($NaHSO_3$, ≥58.5%), ammonium persulfate ($(NH_4)_2S_2O_8$, ≥98.0%), sodium hydroxide (NaOH, ≥96.0%), sodium chloride (NaCl, ≥99.5%), magnesium chloride hexahydrate ($MgCl_2{\cdot}6H_2O$, ≥98.0%), calcium chloride anhydrous ($CaCl_2$, ≥96.0%), potassium chloride (KCl, ≥99.5%), sodium sulfate (Na_2SO_4, ≥99.0%),

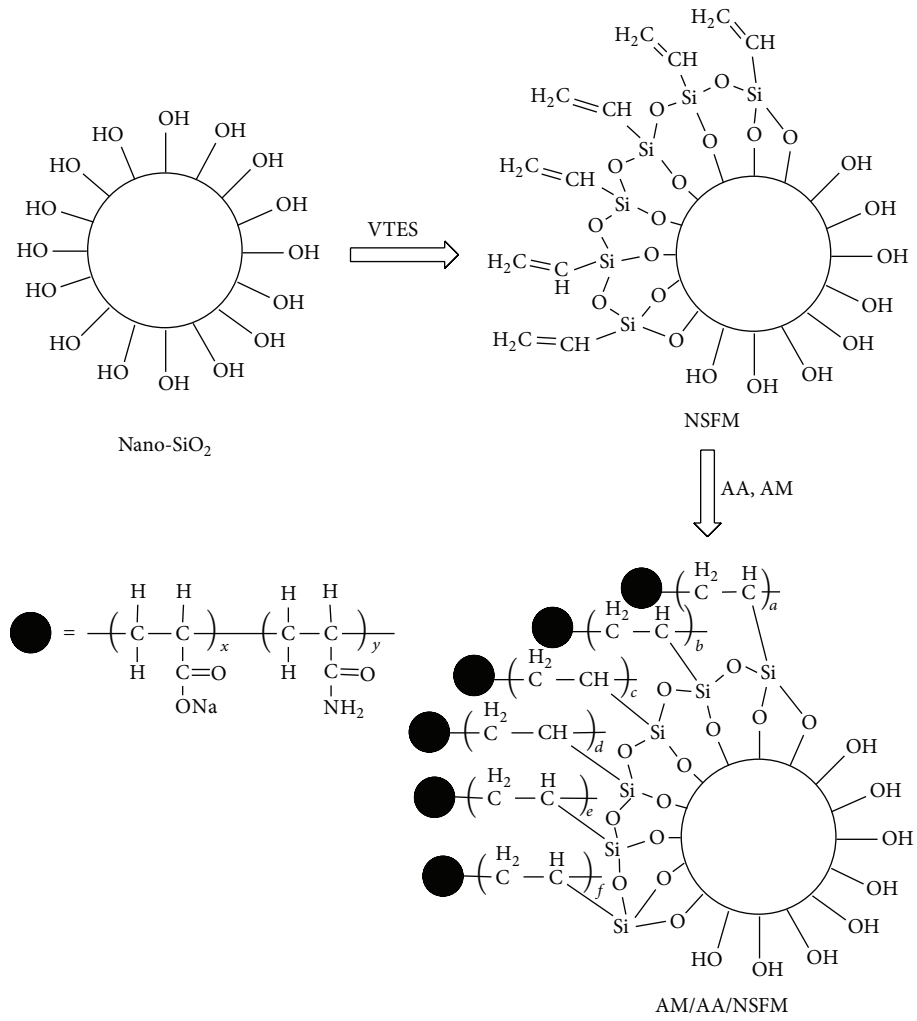

Scheme 1: The synthesis of AM/AA/NSFM.

and sodium bicarbonate ($NaHCO_3$, ≥99.5%) were purchased from Chengdu Kelong Chemical Reagent Factory (Sichuan, China). Nano-SiO_2 (10–20 nm) was obtained from Aladdin chemistry (Shanghai, China) Co., Ltd. All chemicals and reagents were used as received without any further purification. Water was deionized by passing through an ion-exchange column and doubly distilled.

2.2. Preparation of Nano-SiO_2 Functional Monomer. Firstly, 83.6 mL ethanol, 1.5 g nano-SiO_2, 13.6 mL distilled water, and 1.3 mL ammonia were added into a 250 mL round-bottom flask, and the mixture was dispersed with supersonic wave for 30 min. Then 2.0 mL VTES was added into the stirred solution in the round-bottom flask, and the reaction time was 18 h at 30°C. After reaction, the product was NSFM which was separated by centrifugation and washed with distilled water [21–23].

2.3. Synthesis of AM/AA/NSFM. 0.05 g NSFM, 6.50 g AM, 3.45 g AA, and a certain amount of distilled water were added into a 100 mL three-necked flask, respectively, and the pH value of the mixture was regulated to 7.0 using sodium hydroxide solution; then the solution with 20% total monomer mass concentration was prepared. 0.05 g $NaHSO_3$-$(NH_4)_2S_2O_8$ initiator (mol ratio = 1:1) was taken along with distilled water in the three-necked flask assembled with a nitrogen (N_2) inlet. Then the copolymerization was carried out at 45°C under N_2 atmosphere for 6 h. Finally, the AM/AA/NSFM copolymer was obtained after ethanol washing, drying, and pulverizing. The synthesis of AM/AA/NSFM is shown in Scheme 1 [20]. The AM/AA copolymer was synthesized by using the same method.

2.4. Characterization. Infrared (IR) spectra of AM/AA and AM/AA/NSFM were measured with KBr pellets using a Perkin Elemer RX-1 spectrophotometer. ^{1}H NMR spectrum of AM/AA/NSFM was recorded on a Bruker AC-E 200 spectrometer by dissolving the copolymer in D_2O and operating at 400 MHz. The elementary analysis of AM/AA/NSFM was carried out with a Vario EL-III elemental analyzer. The microstructures of AM/AA and AM/AA/NSFM were observed by a scanning electron microscope (SEM). The

Table 1: Composition and TDS of brine.

Composition	NaCl	KCl	$CaCl_2$	$MgCl_2{\cdot}6H_2O$	Na_2SO_4	$NaHCO_3$	TDS
Content (wt%)	0.8495	0.0149	0.0764	0.2154	0.0125	0.0428	1.0951

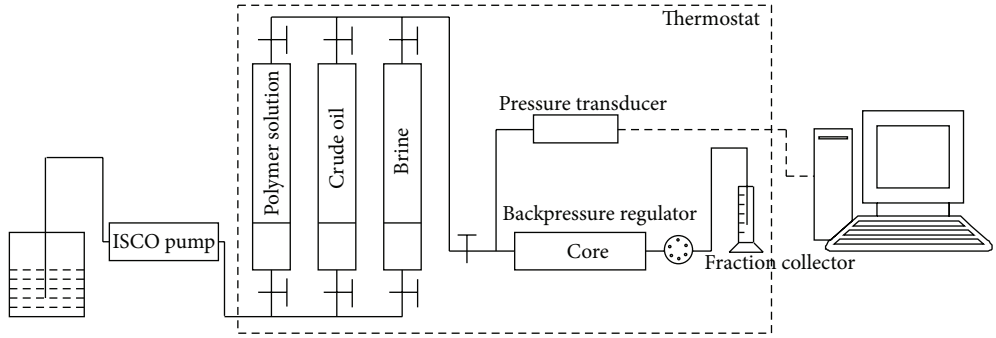

Figure 1: Flow chart of the core flooding experiments.

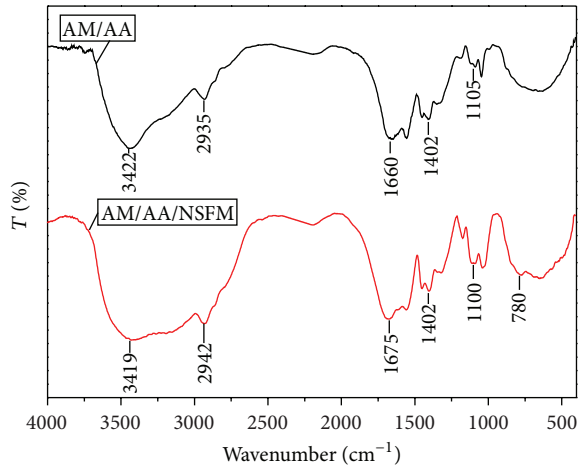

Figure 2: IR spectra of AM/AA and AM/AA/NSFM.

weight-average molecular weight (M_w) of the copolymers was obtained by using a BI-200SM wide angle dynamic/static laser light scattering apparatus.

2.5. Intrinsic Viscosity. The intrinsic viscosity of copolymer was measured with an Ubbelohde viscometer at 25°C. The test temperature was controlled using a constant temperature bath. The flux time was reproducible to 0.05 s using a stopwatch. The copolymer solutions, at five different concentrations (0.1000, 0.0667, 0.0500, 0.0333, and 0.0250 wt%), were prepared with distilled water. The specific viscosity is calculated via the following equation [6, 24, 25]:

$$\eta_{sp} = \frac{t - t_0}{t_0}, \tag{1}$$

where η_{sp} is the specific viscosity of copolymer; t_0 is flux time of distilled water, s; and t is flux time of copolymer solution, s.

Then the intrinsic viscosity is calculated with the Huggins equation [6, 26]:

$$\frac{\eta_{sp}}{C} = [\eta] + K'[\eta]^2 C, \tag{2}$$

where $[\eta]$ is intrinsic viscosity, mL/g; C is concentration of copolymer solution, wt%; and K' is the Huggins constant.

2.6. Rheological Property and Viscoelasticity. Rheological property and viscoelasticity measurements of the copolymers were conducted on a HAAKE RS 600 Rotational Rheometer (Germany). The shear rate was from 0.007 s^{-1} to 500 s^{-1}, and the temperature was 65°C with a heating rate of 1.5°C/min, while the test system was binocular tube and the rotor was DG41Ti in rheological measurements. The scanning range of frequency (f) was 0.01–10 Hz, and the stress was 0.1 Pa by using the same test system and rotor in viscoelasticity measurements.

2.7. Mobility Control Ability. The mobility control ability of the copolymer solutions is characterized by the resistance factor (RF) and the residual resistance factor (RRF) [27–29]. The RF is calculated with the following equation:

$$\mathrm{RF} = \frac{K_w/\mu_w}{K_p/\mu_p}, \tag{3}$$

where K_w is aqueous phase permeability, mD; K_p is polymer phase permeability, mD; μ_w is the viscosity of aqueous phase, mPa·s; and μ_p is the viscosity of polymer phase, mPa·s.

The RRF is calculated with the following equation:

$$\mathrm{RRF} = \frac{K_{wb}}{K_{wa}}, \tag{4}$$

where K_{wb} is aqueous phase permeability before polymer flooding, mD; K_{wa} is aqueous phase permeability after polymer flooding, mD.

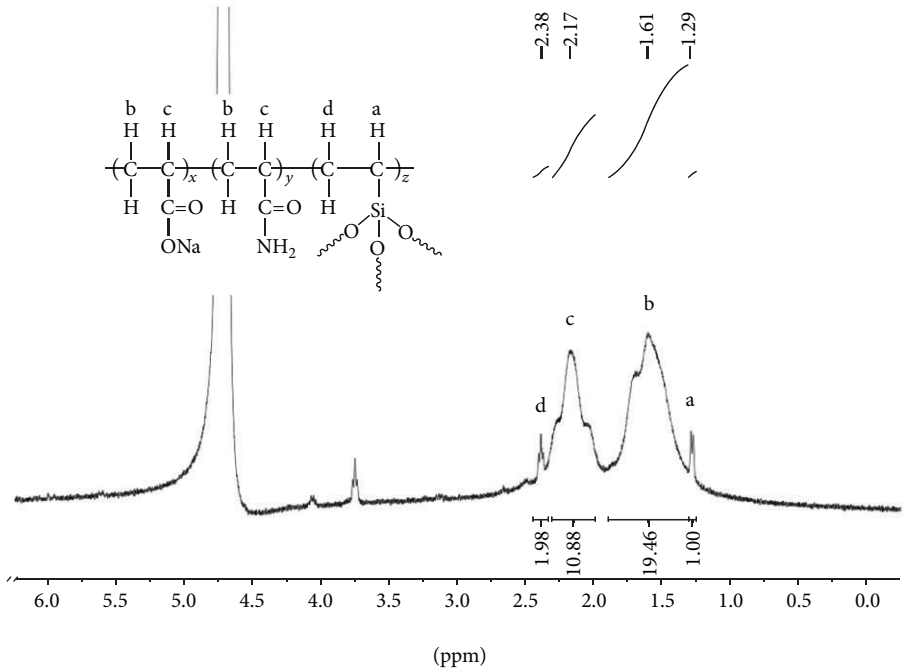

Figure 3: ^{1}H NMR spectrum of AM/AA/NSFM in D_2O.

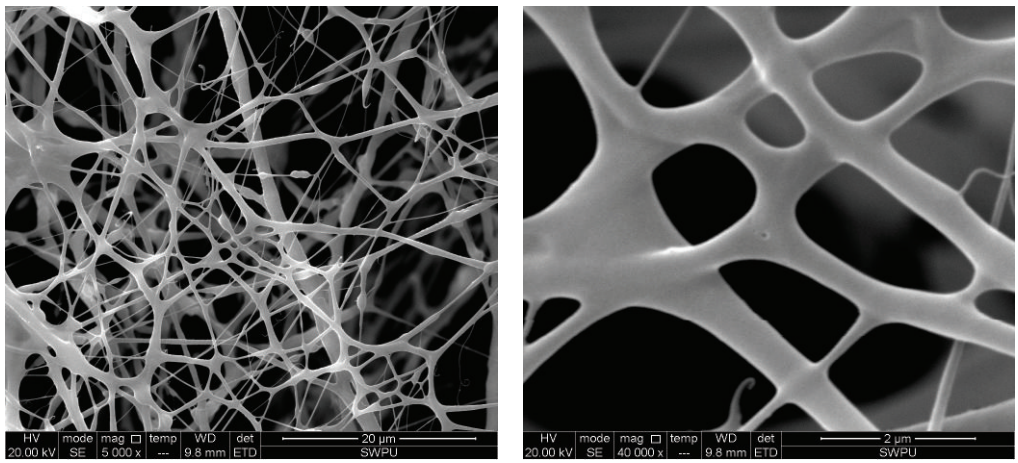

(a) (b)

Figure 4: SEM images of AM/AA.

2.8. Core Flooding Tests. Two Berea sandstone cores were used for core flooding experiments. The cores were dried at 65°C, and then their length, diameter, porosity, and gas permeability were measured by using a SCMS-B2 core multiparameter measurement system. A Hassler core holder was used with 3.5 MPa confining pressure and 1.5 MPa backpressure. The core, after being saturated with brine, was saturated with crude oil (52.5 mPa·s at 65°C) at 0.1-0.2 mL/min until irreducible water saturation (S_{wi}) was obtained. After 72 h of aging, the core was flooded by the brine at 0.2 mL/min until water cut was up to 95%, and then the copolymer solution (0.2 wt%) was injected at 0.2 mL/min until water cut reached 95% once more [6, 29]. All the core flooding procedures were conducted at 65°C. Chemical composition and total dissolved solids (TDS) of the brine are listed in Table 1. The maximum work pressure of the ISCO 260D syringe pump is 50 MPa, and its minimum and maximum displacement velocity is 0.001 and 50.000 mL/min, respectively. The EOR is calculated with the following equation:

$$\text{EOR} = E - E_w, \tag{5}$$

where EOR is enhanced oil recovery, %; E is the oil recovery of the whole displacement process, %; and E_w is the oil recovery of water flooding, %.

Flow chart of the core flooding experiments is shown in Figure 1.

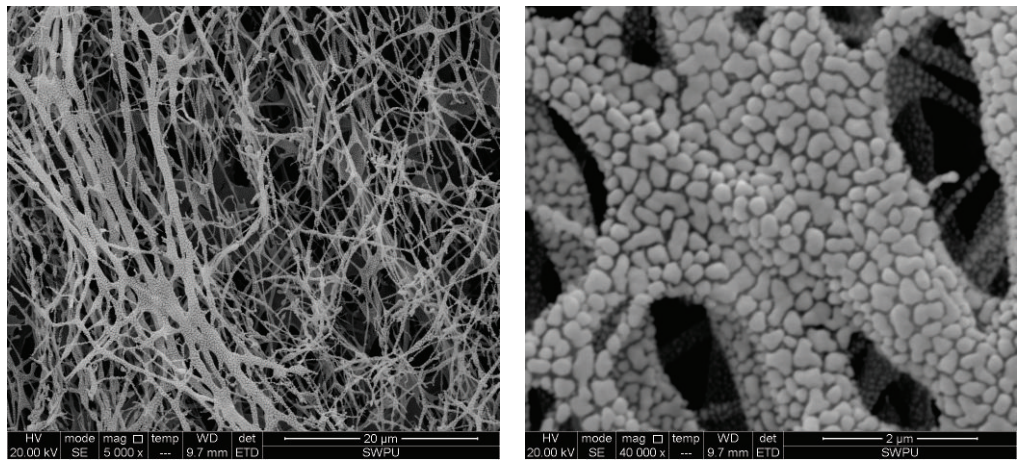

(a) (b)

Figure 5: SEM images of AM/AA/NSFM.

Table 2: The relevant core properties and the results of core flooding experiments.

Copolymer	Cores	Length (cm)	Diameter (cm)	Porosity (%)	Permeability (mD)	S_{wi} (%)	E (%)	E_w (%)	EOR (%)
AM/AA	1#	8.84	3.77	23.11	937.03	19.18	45.73	31.51	14.22
AM/AA/NSFM	2#	8.92	3.78	23.05	926.28	19.37	52.85	31.75	20.10

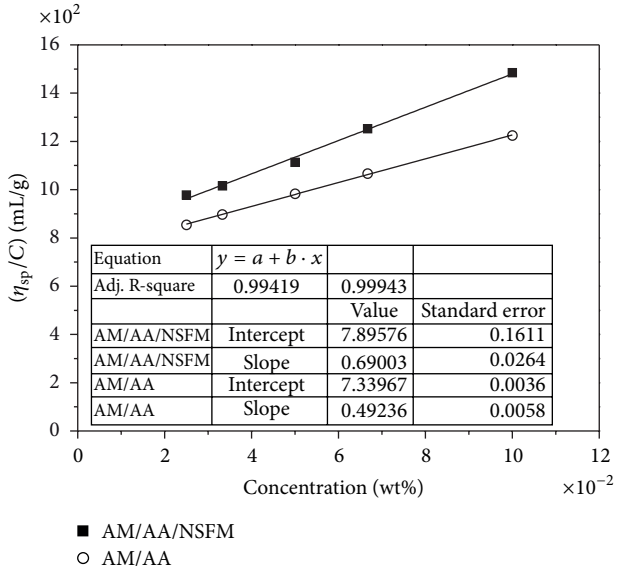

Figure 6: The η_{sp}/C versus C relationships of AM/AA and AM/AA/NSFM.

3. Results and Discussion

3.1. IR Spectra Analysis. The structures of AM/AA and AM/AA/NSFM were confirmed by IR spectra as illustrated in Figure 2. The AM/AA/NSFM which was prepared using acrylic acid, acrylamide, and NSFM by free radical polymerization was confirmed by strong absorptions at 3419 cm^{-1} (–NH stretching vibration and –OH stretching vibration), 2942 cm^{-1} (–CH_2 stretching vibration), 1675 cm^{-1} (C=O stretching vibration), 1402 cm^{-1} (C–N stretching vibration), 1100 cm^{-1} (Si–O–Si asymmetric stretching vibration), and 780 cm^{-1} (Si–O–Si symmetric stretching vibration) in the spectrum of AM/AA/NSFM [18, 20]. The peak at 3419 cm^{-1} was broad in the IR spectrum of AM/AA/NSFM partly due to the hydroxyl on nano-SiO_2 surface [20]. As expected, the IR spectra confirmed the presence of different monomers in AM/AA/NSFM.

3.2. ^1H NMR Analysis. The ^1H NMR spectrum of AM/AA/NSFM is shown in Figure 3. The chemical shift value at 1.29 ppm is due to the protons of [–CH_2–C**H** (Si(O–)$_3$)–]. The chemical shift value at 1.61 ppm is assigned to the protons of [–C**H**$_2$–CH ($CONH_2$)–] and [–C**H**$_2$–CH (COONa)–]. The protons of [–CH_2–C**H** ($CONH_2$)–] and [–CH_2–C**H** (COONa)–] appear at 2.17 ppm. The characteristic peak due to the protons of [–C**H**$_2$–CH (Si(O–)$_3$)–] is observed at 2.38 ppm.

3.3. Elementary Analysis of AM/AA/NSFM. The elementary analysis of the AM/AA/NSFM copolymer was carried out using a Vario EL-III elemental analyzer. The content of different element in the copolymer can be obtained by detecting the gases, which are the decomposition products of the copolymer at high temperature. Theoretical value: 0.21% (Si %), 45.4% (C %), and 5.4% (H %); found value: 0.17% (Si %), 40.1% (C %), and 4.8% (H %).

3.4. Microscopic Structure. The microscopic structures of AM/AA and AM/AA/NSFM were observed through SEM at room temperature. The copolymers solution samples

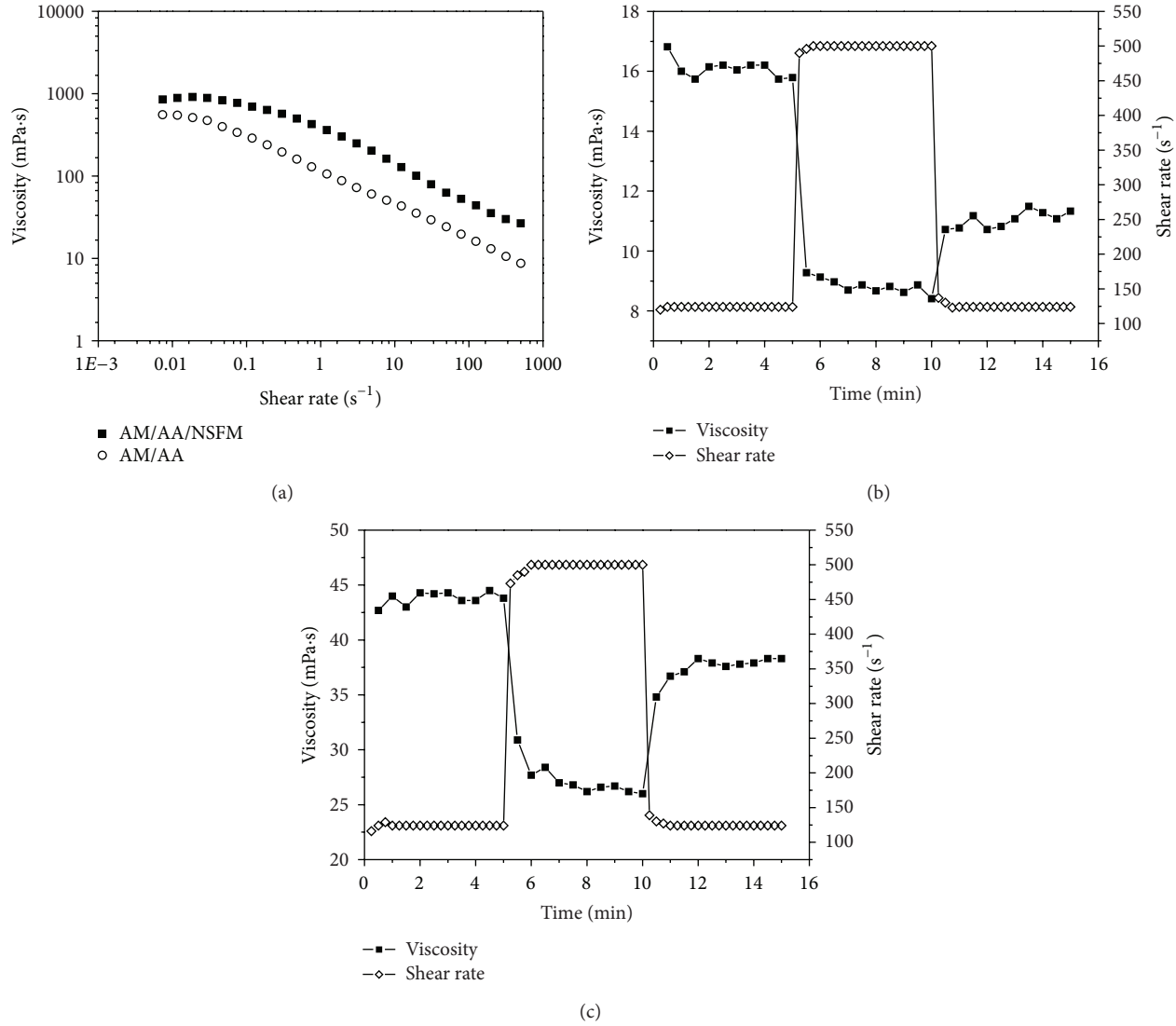

FIGURE 7: (a) Effect of shear rate on viscosity; (b) shear resistance of AM/AA; (c) shear resistance of AM/AA/NSFM. The copolymers solutions (0.2 wt%) were prepared with distilled water.

(0.05 wt%) were prepared with distilled water and cooled with liquid nitrogen, and then these samples were evacuated in order to keep original appearance of the copolymers as far as possible. As shown in Figures 4 and 5, the molecular chains of copolymer were obviously changed when NSFM was introduced into the AM/AA copolymer. Compared with the images of AM/AA, the molecular coils of AM/AA/NSFM were composed of many micro-nano structure units, and the force between these units could be heightened due to Si–O and C–Si bonds. In addition, this structure may increase retention of AM/AA/NSFM on the rock face which is favorable to mobility control and EOR.

3.5. Weight-Average Molecular Weight. Five different concentrations (0.001, 0.002, 0.004, 0.006, and 0.008 wt%) copolymer solutions were prepared with distilled water and filtered using a 0.5 μm Millipore Millex-LCR filter before static laser light scattering (SLLS) experiments. The M_w of AM/AA and AM/AA/NSFM can be calculated with the following equation [30]:

$$\frac{KC}{R_{vv}(q)} \cong \frac{1}{M_w}\left(1 + \frac{1}{3}\left\langle R_g\right\rangle^2 q^2\right), \tag{6}$$

where K is a constant; C is the concentration of copolymer solution, g/mL; $R_{vv}(q)$ is the Rayleigh ratio; $\langle R_g\rangle$ is the average radius of gyration, nm; and $q = (4\pi n/\lambda_o)\sin(\theta/2)$ with θ, λ_o, and n being the scattering angle, the wavelength of light in vacuo, and the solvent refractive index, respectively.

The M_w of AM/AA and AM/AA/NSFM is (1.33 ± 0.30) × 10^7 g/mol and (1.32 ± 0.45) × 10^7 g/mol, respectively (for details, see Supporting Material available online at http://dx.doi.org/10.1155/2013/437309).

3.6. Intrinsic Viscosity. The η_{sp}/C versus C relationship is shown in Figure 6. The fitted line of η_{sp}/C versus C was

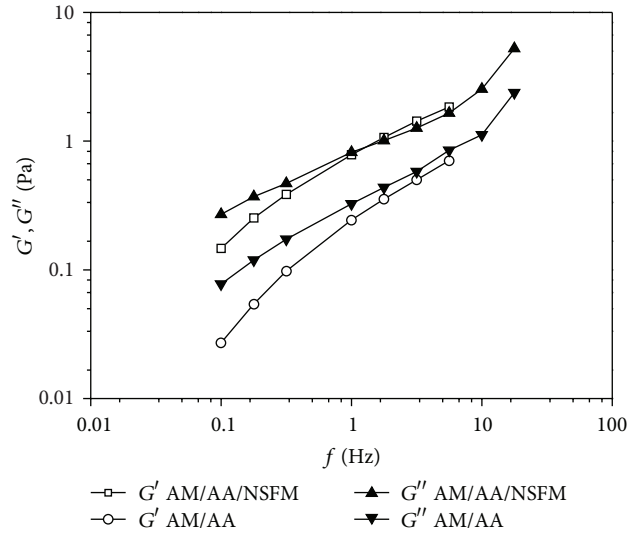

Figure 8: Viscoelasticity of AM/AA and AM/AA/NSFM at 65°C. The copolymers solutions (0.2 wt%) were prepared with distilled water.

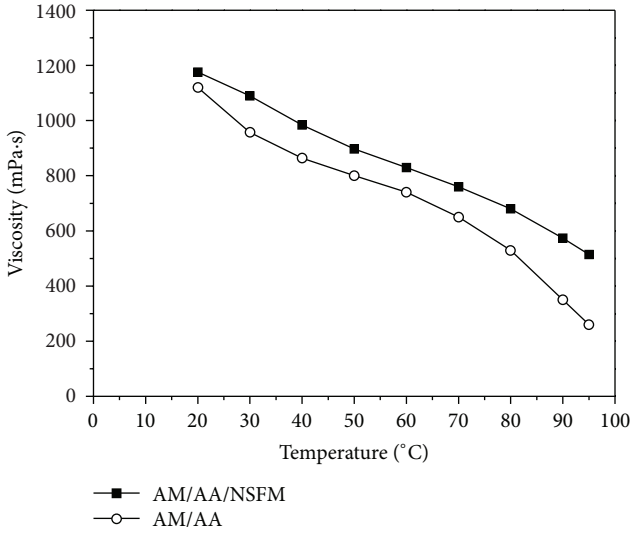

Figure 9: Viscosity versus temperature for AM/AA and AM/AA/NSFM solution. The viscosity of copolymer solution (0.5 wt%) was measured by Brookfiled DV-3 viscometer at 7.34 s^{-1} using number 62 rotor (rotation speed: 18.8 r/min).

extrapolated to zero concentration. According to the Huggins equation, the y-intercept is the intrinsic viscosity of the copolymers. The results revealed that the intrinsic viscosity of AM/AA and AM/AA/NSFM was 733.9 and 789.5 mL/g, respectively.

3.7. Shear Resistance. The viscosity versus shear rate curves of AM/AA and AM/AA/NSFM (0.2 wt%) are shown in Figure 7(a). It was clearly found that AM/AA and AM/AA/NSFM revealed non-Newtonian shear-thinning behavior. Hence, with the increase of the shear rate (from 0.007 to 500 s^{-1}), the viscosity of copolymer solutions dropped obviously. The results indicated that AM/AA/NSFM had better viscosifying property than AM/AA, and the viscosity of AM/AA/NSFM was higher than that of AM/AA at 500 s^{-1} shear rate (18.6 mPa·s versus 8.7 mPa·s). Furthermore, AM/AA and AM/AA/NSFM were investigated by changing the shear rate from 124 s^{-1} to 500 s^{-1} and from 500 s^{-1} to 124 s^{-1} around (Figures 7(b) and 7(c)). Compared with AM/AA, AM/AA/NSFM had higher retention rate of viscosity (85% versus 68%) when one cycle was completed. This phenomenon may support the Si–O and C–Si bonds in AM/AA/ NSFM which can improve the shear tolerance of the copolymer. The structures of AM/AA/NSFM may be restored after being sheared.

3.8. Viscoelasticity Measurements. The viscoelasticity curves of AM/AA and AM/AA/NSFM solutions (0.2 wt%) are shown in Figure 8. When the frequency was lower than 1 Hz, the viscous modulus (G'') of AM/AA/NSFM was higher than the elastic modulus (G'); when the frequency was higher than 1 Hz, the situation was just the opposite. However, the G'' of AM/AA was higher than G' in the entire frequency scan range. Compared with AM/AA, AM/AA/NSFM exhibited higher G' and G'' under the same conditions. This phenomenon may support the micro-nano structure units in AM/AA/NSFM can enhance the acting force of polymer molecular coils.

3.9. Temperature Tolerance. AM/AA and AM/AA/NSFM solutions were prepared with distilled water. And the viscosity of copolymer solutions was measured by the Brookfiled DV-3 viscometer at different temperatures. The viscosity versus temperature curves of AM/AA and AM/AA/NSFM solutions are shown in Figure 9. The test results showed that the AM/AA/NSFM solution had higher viscosity at the same temperature. Additionally, the viscosity of AM/AA/NSFM solution decreased less than that of AM/AA when temperature was above 80°C. This may support the stable Si–O and C–Si bonds which can obviously improve temperature tolerance of AM/AA/NSFM.

3.10. Salt Tolerance. As shown in Figures 10(a), 10(b), and 10(c), with the increase of salt concentration (NaCl, $CaCl_2$, and $MgCl_2{\cdot}6H_2O$), the viscosity of copolymers decreases rapidly and then kept at a low value. It was found that AM/AA and AM/AA/NSFM had less satisfactory salt tolerance to Na^+ or Ca^{2+} than to Mg^{2+} under the same conditions. Compared with AM/AA, AM/AA/NSFM exhibited no obvious advantage in salt tolerance due to the shrinking of copolymer chain with the increase of salt concentration.

3.11. Mobility Control Ability. The core barrel was packed with quartz sand which was washed by hydrochloric acid and distilled water for several times. The injection rate of brine (sodium chloride concentration was 0.5 wt%) and polymer solution prepared with the brine was 2.0 mL/min with the ISCO 260D syringe pump. Experiments were carried out at 65°C in an incubator with precision of 0.1°C. The injection

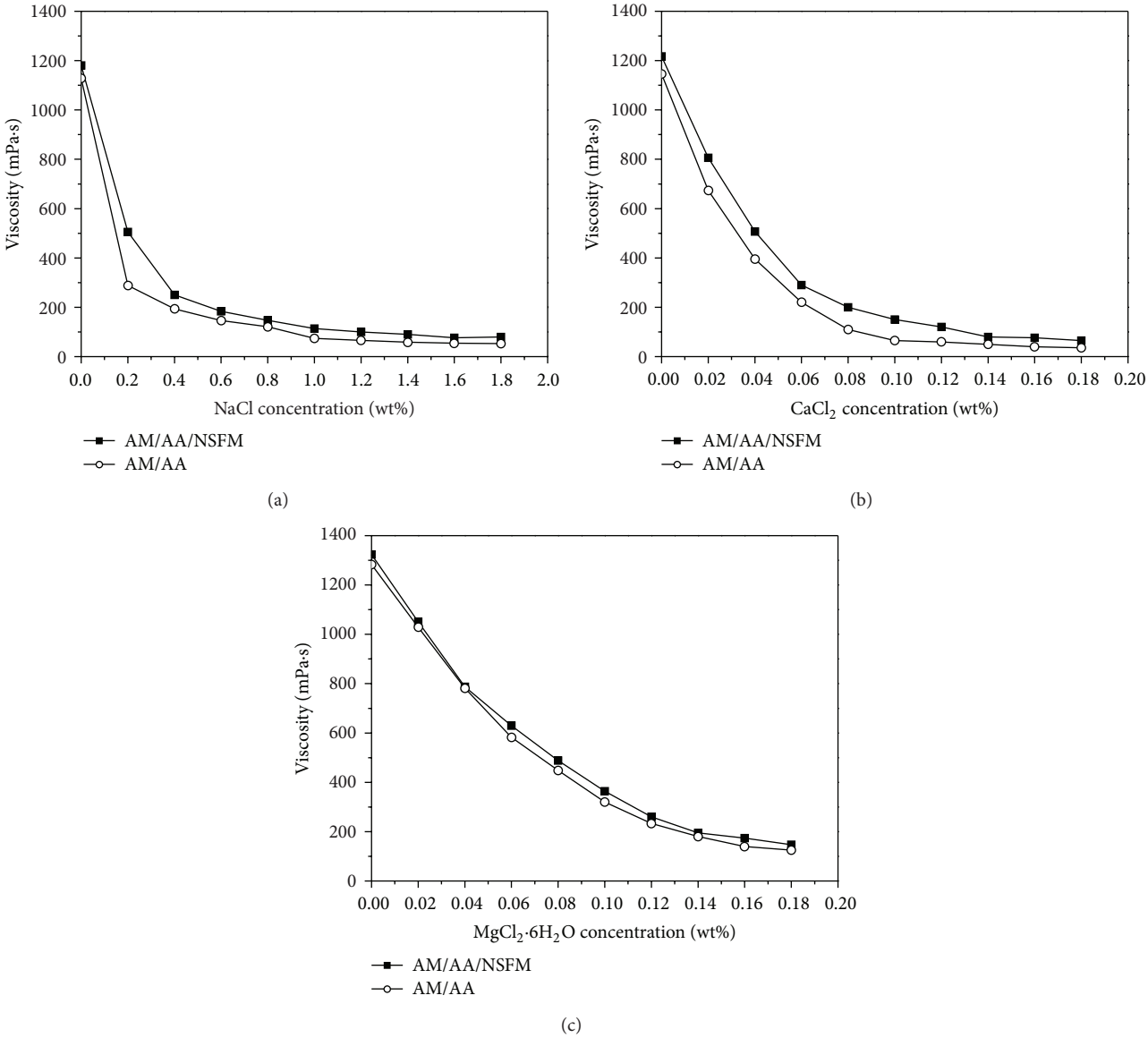

Figure 10: Salt tolerance ((a) NaCl, (b) $CaCl_2$, and (c) $MgCl_2 \cdot 6H_2O$) of AM/AA and AM/AA/NSFM solutions (0.5 wt%) at 20°C. The viscosity of copolymer solution was measured by Brookfiled DV-3 viscometer at 7.34 s^{-1} using number 62 rotor (rotation speed: 18.8 r/min) or number 61 rotor (rotation speed: 18.5 r/min).

pressure was collected by a pressure sensor with precision of 0.0001 MPa. The flow characteristic curves of AM/AA and AM/AA/NSFM in porous media are shown in Figure 11.

As shown in Figure 11, the AM/AA/NSFM solution could establish much higher RF and RRF than that of the AM/AA solution under the same conditions (RF: 16.52 versus 12.17, RRF: 3.63 versus 2.59). This is to say that the AM/AA/NSFM solution has stronger mobility control ability which is favorable to enhance oil recovery due to the higher viscosity retention rate and microstructure. In addition, it was found that AM/AA/NSFM revealed higher retention than AM/AA (83 mg versus 55 mg) by material balance calculations (for details, see Supporting Materials). This may support that the huge surface area of micro-nano structure units of AM/AA/NSFM can enhance the adsorption which may play an important role in improving mobility control.

3.12. Enhanced Oil Recovery. As shown in Table 2, the EOR of AM/AA/NSFM solution (0.2 wt%) was 20.10% compared with water flooding at 65°C. However, the EOR of AM/AA solution (0.2 wt%) was 14.22% under the same conditions. The EOR results showed that AM/AA/NSFM revealed more superior ability of oil displacement. As shown in Figure 12, compared with AM/AA, AM/AA/NSFM exhibited stronger ability of reducing water cut and establishing flow resistance in polymer flooding process. This phenomenon may support that the sweep efficiency is obviously improved

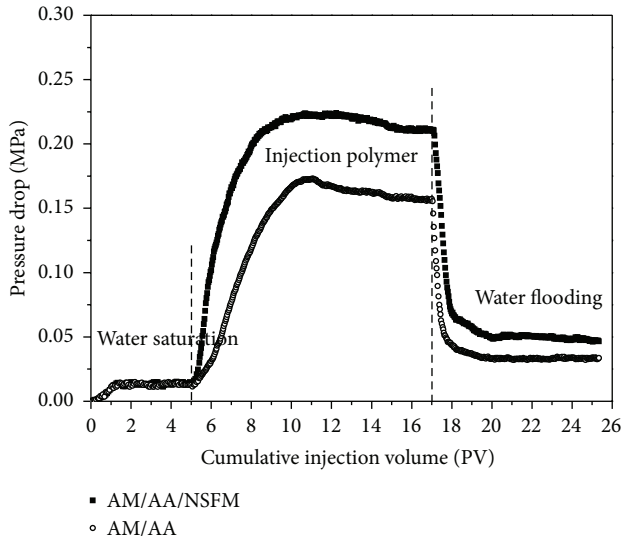

Figure 11: Flow characteristic curves of AM/AA and AM/AA/NSFM solution (0.2 wt%). The length and internal diameter of the core barrel were 25.0 cm and 2.5 cm, respectively.

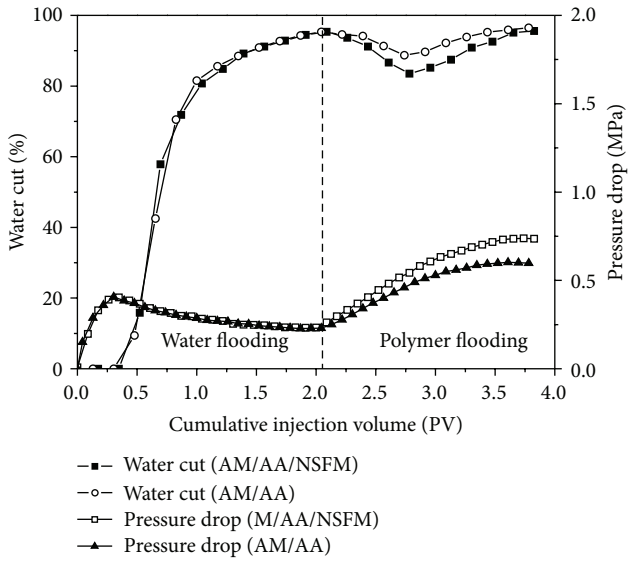

Figure 12: Core flooding experiments results of AM/AA/NSFM and AM/AA (0.2 wt%) at 65°C.

by AM/AA/NSFM due to the excellent mobility control capability in porous media.

4. Conclusions

A novel copolymer containing nano-SiO_2 was synthesized by free radical polymerization using AM, AA, and NSFM as raw materials. The AM/AA/NSFM copolymer was characterized by IR spectrum, ^{1}H NMR spectrum, elemental analysis, and scanning electron microscope. The solution properties, such as rheological property, viscoelasticity, temperature tolerance, salt tolerance, mobility control ability, and oil displacement efficiency of the copolymer, were investigated under different conditions. The results indicated that the copolymer containing nano-SiO_2 possessed moderate or good shear resistance, temperature tolerance, and mobility control ability as EOR chemical.

Conflict of Interests

The authors declare no possible conflict of interests.

Acknowledgments

This work was supported by the Open Fund (PLN1212) of State Key Laboratory of Oil and Gas Reservoir Geology and Exploitation (Southwest Petroleum University) and the Specialized Research Fund for the Doctoral Program of Higher Education (20125121120011).

References

[1] N. Mungan, F. W. Smith, J. L. Thompson, O. Sinclair, and C. Gas, "Some aspects of polymer floods," *Journal of Petroleum Technology*, vol. 18, no. 9, pp. 1143–1150, 1966.

[2] B. S. Shiran and A. Skauge, "Enhanced oil recovery (EOR) by combined low salinity water/polymer flooding," *Energy Fuels*, vol. 27, no. 3, pp. 1223–1235, 2013.

[3] C. Zhong, R. Huang, X. Zhang, and H. Dai, "Synthesis, characterization, and solution properties or an acrylamide-based terpolymer with butyl styrene," *Journal of Applied Polymer Science*, vol. 103, no. 6, pp. 4027–4038, 2007.

[4] T. Rho, J. Park, C. Kim, H. Yoon, and H. Suh, "Degradation of polyacrylamide in dilute solution," *Polymer Degradation and Stability*, vol. 51, no. 3, pp. 287–293, 1996.

[5] D. A. Z. Wever, F. Picchioni, and A. A. Broekhuis, "Polymers for enhanced oil recovery: a paradigm for structure-property relationship in aqueous solution," *Progress in Polymer Science*, vol. 36, no. 11, pp. 1558–1628, 2011.

[6] Z. B. Ye, G. J. Gou, S. H. Gou, W. C. Jiang, and T. Y. Liu, "Synthesis and characterization of a water-soluble sulfonates copolymer of acrylamide and N-Allylbenzamide as enhanced oil recovery chemical," *Journal of Applied Polymer Science*, vol. 128, no. 3, pp. 2003–2011, 2013.

[7] S. H. Chang and I. J. Chung, "Effect of shear flow on polymer desorption and latex dispersion stability in the presence of adsorbed polymer," *Macromolecules*, vol. 24, no. 2, pp. 567–571, 1991.

[8] L. Xue, U. S. Agarwal, and P. J. Lemstra, "Shear degradation resistance of star polymers during elongational flow," *Macromolecules*, vol. 38, no. 21, pp. 8825–8832, 2005.

[9] J. Zheng, P. Cui, X. Tian, and K. Zheng, "Pyrolysis studies of polyethylene terephthalate/silica nanocomposites," *Journal of Applied Polymer Science*, vol. 104, no. 1, pp. 9–14, 2007.

[10] L. I. Rueda, L. G. Hernandez, and C. C. Anton, "Effect of the textural characteristics of the new silicas on the dynamic properties of Styrene-Butadiene Rubber (SBR) vulcanizates," *Polymer Composites*, vol. 9, no. 3, pp. 204–208, 1988.

[11] H. Xia and Q. Wang, "Preparation of conductive polyaniline/nanosilica particle composites through ultrasonic irradiation," *Journal of Applied Polymer Science*, vol. 87, no. 11, pp. 1811–1817, 2003.

[12] X. Wang, X. Zhao, M. Wang, and Z. Shen, "The effects of atomic oxygen on polyimide resin matrix composite containing nano-silicon dioxide," *Nuclear Instruments and Methods in Physics Research B*, vol. 243, no. 2, pp. 320–324, 2006.

[13] Y. Li, J. Yu, and Z. Guo, "The influence of interphase on nylon-6/nano-SiO_2 composite materials obtained from in situ polymerization," *Polymer International*, vol. 52, no. 6, pp. 981–986, 2003.

[14] V. A. Bershtein, L. M. Egorova, P. N. Yakushev, P. Pissis, P. Sysel, and L. Brozova, "Molecular dynamics in nanostructured polyimide-silica hybrid materials and their thermal stability," *Journal of Polymer Science B*, vol. 40, no. 10, pp. 1056–1069, 2002.

[15] N. D. Alberola, K. Benzarti, C. Bas, and Y. Bomal, "Interface effects in elastomers reinforced by modified precipitated silica," *Polymer Composites*, vol. 22, no. 2, pp. 312–325, 2001.

[16] A. Voronov, A. Kohut, A. Synytska, and W. Peukert, "Mechanochemical modification of silica with poly(1-vinyl-2-pyrrolidone) by grinding in a stirred media mill," *Journal of Applied Polymer Science*, vol. 104, no. 6, pp. 3708–3714, 2007.

[17] H. Zou, S. Wu, and J. Shen, "Polymer/silica nanocomposites: preparation, characterization, propertles, and applications," *Chemical Reviews*, vol. 108, no. 9, pp. 3893–3957, 2008.

[18] G. Hsiue, W. Kuo, Y. Huang, and R. Jeng, "Microstructural and morphological characteristics of PS-SiO_2 nanocomposites," *Polymer*, vol. 41, no. 8, pp. 2813–2825, 2000.

[19] W. Wang and B. Gu, "Self-assembly of two- and three-dimensional particle arrays by manipulating the hydrophobicity of silica nanospheres," *Journal of Physical Chemistry B*, vol. 109, no. 47, pp. 22175–22180, 2005.

[20] B. J. Kim and K. S. Kang, "Fabrication of a crack-free large area photonic crystal with colloidal silica spheres modified with vinyltriethoxysilane," *Crystal Growth & Design*, vol. 12, no. 8, pp. 4039–4042, 2012.

[21] A. V. Biradar, A. A. Biradar, and T. Asefa, "Silica-dendrimer core-shell microspheres with encapsulated ultrasmall palladium nanoparticles: efficient and easily recyclable heterogeneous nanocatalysts," *Langmuir*, vol. 27, no. 23, pp. 14408–14418, 2011.

[22] Z. Meng, C. Xue, Q. Zhang, X. Yu, K. Xi, and X. Jia, "Preparation of highly monodisperse hybrid silica nanospheres using a one-step emulsion reaction in aqueous solution," *Langmuir*, vol. 25, no. 14, pp. 7879–7883, 2009.

[23] Z. Wu, H. Han, W. Han, B. Kim, K. H. Ahn, and K. Lee, "Controlling the hydrophobicity of submicrometer silica spheres via surface modification for nanocomposite applications," *Langmuir*, vol. 23, no. 14, pp. 7799–7803, 2007.

[24] A. Mehrdad and R. Akbarzadeh, "Effect of temperature and solvent composition on the intrinsic viscosity of poly(vinyl pyrrolidone) in water-ethanol solutions," *Journal of Chemical and Engineering Data*, vol. 55, no. 9, pp. 3720–3724, 2010.

[25] J. Lee and A. Tripathi, "Intrinsic viscosity of polymers and biopolymers measured by microchip," *Analytical Chemistry*, vol. 77, no. 22, pp. 7137–7147, 2005.

[26] L. Alagha, S. Wang, Z. Xu, and J. Masliyah, "Adsorption kinetics of a novel organic-inorganic hybrid polymer on silica and alumina studied by quartz crystal microbalance," *Journal of Physical Chemistry C*, vol. 115, no. 31, pp. 15390–15402, 2011.

[27] R. Ponnapati, O. Karazincir, E. Dao, R. Ng, K. K. Mohanty, and R. Krishnamoorti, "Polymer-functionalized nanoparticles for improving waterflood sweep efficiency: characterization and transport properties," *Industrial and Engineering Chemistry Research*, vol. 50, no. 23, pp. 13030–13036, 2011.

[28] C. Zhong, L. Ye, H. Dai, and R. Huang, "Flourescent probe and ESEM morphologies of a acrylamide-based terpolymer in aqueous solution," *Journal of Applied Polymer Science*, vol. 103, no. 1, pp. 277–286, 2007.

[29] L. Shi, Z. Ye, Z. Zhang, C. Zhou, S. Zhu, and Z. Guo, "Necessity and feasibility of improving the residual resistance factor of polymer flooding in heavy oil reservoirs," *Petroleum Science*, vol. 7, no. 2, pp. 251–256, 2010.

[30] X. Wang, X. Qiu, and C. Wu, "Comparison of the coil-to-globule and the globule-to-coil transitions of a single poly(N-isopropylacrylamide) homopolymer chain in water," *Macromolecules*, vol. 31, no. 9, pp. 2972–2976, 1998.